JOURNAL OF MATERIALS SCIENCE 23 (1988) 4429–4436

A structural study on solid state drawing of solution-crystallized ultra-high molecular weight polyethylene

N. A. J. M. VAN AERLE
Department of Polymer Technology, Eindhoven University of Technology, P.O. Box 513, 5600 MB Eindhoven, The Netherlands

A. W. M. BRAAM
DSM Research, P.O. Box 18, 6160 MD Geleen, The Netherlands

The influence of solid state drawing of solution-crystallized ultra-high molecular weight polyethylene on the structure has been studied. Results obtained by different wide-angle and small-angle X-ray techniques support a deformation mechanism, which was partially described by Peterlin. An extended mechanism is proposed, which not only explains the orientational effects observed via WAXS and SAXS fairly easily, but can also account for the constancy of the long period, the steady decrease of the meridional SAXS intensity, the increase in crystallinity and the increase in the longitudinal crystallite size as the draw ratio increases (starting from a draw ratio of 10). Furthermore, the observed changes in lateral apparent crystal sizes as well as the stress–strain behaviour during the drawing process can be understood easily in terms of this model.

1. Introduction

Conventional semi-crystalline polymers exhibit tensile strengths and Young's moduli considerably lower than their theoretically achievable values. Many researchers have tried to bridge this gap. For flexible polymers like polyethylene and polypropylene it is well known that the introduction of molecular orientation, e.g. by uniaxial drawing, decreases the difference between the theoretical and experimental mechanical properties.

In the late seventies Smith *et al.* [1–7] introduced a method of obtaining ultra-high molecular orientation in polyethylene. Their method consists of crystallizing ultra-high molecular weight polyethylene (UHMW-PE) from a semi-dilute solution. The resulting gels – after evaporation of the solvent – can be drawn to very high draw ratios, leading to ultra-oriented fibres or tapes with excellent mechanical properties.

At the time, no straightforward explanation of such extraordinary orientations and related properties was available. In addition, no adequate experimental results on the structure of the final ultra-drawn materials were available. Smith *et al.* studied the structure and texture of the undrawn gels by means of scanning electron microscopy (SEM) and wide angle X-ray scattering (WAXS) [2, 7]. They showed that the gels – after removal of the solvent – consisted of partially oriented conglomerates of lamellae with some preferential orientation. In a similar way they studied the structure of the ultra-drawn samples and proved the existence of extreme anisotropy. However, they were not able to describe the structure of the ultra-drawn samples in sufficient detail to explain the mechanical properties achieved. Only very recently has high-resolution electron microscopy been performed on ultra-drawn UHMW-PE [8].

Several deformation mechanisms have been proposed in the past to describe the morphological changes during drawing of flexible semi-crystalline-polymers. One of the first deformation models was proposed by Kobayashi [9]. He assumed a complete unfolding of molecules in the necking region. However, most of the experimental results support the currently accepted deformation mechanism of Peterlin [10–16]. In this model a large scale irreversible deformation of PE involves sliding and tilting of lamellae, resulting in the formation of crystalline blocks. These crystalline blocks organize into so-called microfibrils. Further deformation leads to shearing of the microfibrils and to chain extension of inter-microfibrillar tie molecules. This deformation model has been disputed by several authors [17–22]. Some of them have proposed a temporary melting during the first stages of drawing [19–22]. The strongest and often-cited evidence for melting and recrystallization on drawing is the correlation between the long period (measured via small angle X-ray scattering (SAXS)) and the drawing temperature, which is independent of the initial lamellar thickness [23]. However, as long as high randomization of molecules is prevented by applied stress, no significant influence of possible partial melting on the deformation phenomena is to be expected. Especially since the lifetime of such a temporary melt, generated via the drawing process, will be quite short.

0022–2461/88 $03.00 + .12

The Peterlin model has often been used to describe experimental results of deformation studies of melt-crystallized samples of polyethylene. However, as far as we know, the structural changes of gel-cast PE have never been studied in detail before.

To get a better insight into the deformation and the final structure of the ultra-drawn material, extensive X-ray scattering experiments (WAXS and SAXS) have been carried out, the results of which will be reported here. All measurements were carried out at room temperature on samples drawn at elevated temperatures to different draw ratios.

2. Experimental procedure

2.1. Sample preparation

2 wt % UHMW-PE gels (Hostalen GUR-412, Hoechst/Ruhrchemie, Mw = 1500 kg mol^{-1}) were prepared as described in the literature [24]. The solvent was evaporated in a fume cupboard at room temperature. Drawn tapes were obtained by stretching dried gel to the desired draw ratio at 120° C with an Instron-1195. The stretching velocity was chosen to be 100 mm min^{-1}. Ink marks were used to determine the draw ratio after the necking region. Since the used PE-gels neck during the first drawing stages, the draw ratio within the necking region changes quite drastically from 1.2 to about 5 within a range of less than 1.5 mm sample length. In this region the draw ratio was determined by measuring the change in cross-section area with an optical microscope, assuming preservation of polymer volume.

2.2. Techniques

Most of the WAXS and SAXS data were obtained simultaneously with a Kiessig camera, using nickel-filtered Cu$K\alpha$-radiation generated by a Nonius Diffractis Generator operating at 40 kV and 26 mA. The sample to film distance was 400 mm for SAXS and 67 mm for WAXS. For the X-ray results in the necking region the Kiessig camera was equipped with a very fine pinhole collimation set to reduce the exposed area. Simultaneous detection of the WAXS and SAXS patterns ensures detection of both characteristics at exactly the same sample area.

For more precise and quantitative SAXS results a Kratky camera with a line focus of 0.1 × 20 mm^2 was used with nickel-filtered Cu$K\alpha$-radiation generated by a Philips PW1130 generator operating at 45 kV and 35 mA. The scattering intensities were recorded photographically (D7 Agfa Gevaert film) and measured with an Enraf Nonius micro-densitometer model 1 [25]. The sample to film distance varied between 200 and 230 mm. Finally, the data were manipulated with the program FFSAXS [26], using computers from the Univac 1100 series. Some additional WAXS data were recorded with a flat film camera, choosing a sample to film distance of 27 mm.

Line-broadening effects, to determine apparent crystal sizes (ACS), were recorded photographically with a Guinier camera, using X-ray generating conditions as for the Kiessig camera. Instrumental broadening was corrected for using a thin film of Al_2O_3 powder (with crystal sizes of more than 100 nm). The halfwidths of the diffraction peaks were calculated, assuming a Gaussian profile, with

$$\Delta\beta^2_{obs} = \Delta\beta^2_s + \Delta\beta^2_i \quad (1)$$

in which $\Delta\beta_{obs}$ is the observed peak width at half-maximum intensity, $\Delta\beta_s$ the broadening caused by the crystallites within the sample and $\Delta\beta_i$ the instrumental line broadening, which appeared to be 0.15°. The broadening effects were interpreted as the ACS and calculated via the Scherrer equation

$$D_{hkl} = K \cdot \lambda_x/(\Delta\beta_s \cos(\theta_{hkl})) \quad (2)$$

in which D_{hkl} is the ACS along the $h\,k\,l$ direction, $2\theta_{hkl}$ the corresponding Bragg reflection angle, λ_x the wavelength of the X-ray source (0.1542 nm) and K a constant chosen to be 0.9.

3. Results

3.1. Undrawn gel

In Fig. 1 some X-ray patterns in combination with a schematic representation of the initial undrawn PE-gel are presented, showing that both the long-range order and the molecular chain orientation are anisotropic with respect to the gel surface. As can be seen, the long-range periodicity as well as the molecular chain direction are, on average, perpendicular to the gel surface (the XY plane in Fig. 1). However, the a and b axes of the crystallites are distributed at random in the plane parallel to the gel surface. The appearance of higher order SAXS reflections, as can be detected by choosing longer exposure times (not shown here) implies a fairly high degree of long-range ordering.

3.2. Structure of drawn gels (tapes)

The structural changes occurring during drawing were studied by recording the structural parameters at different draw ratios at room temperature.

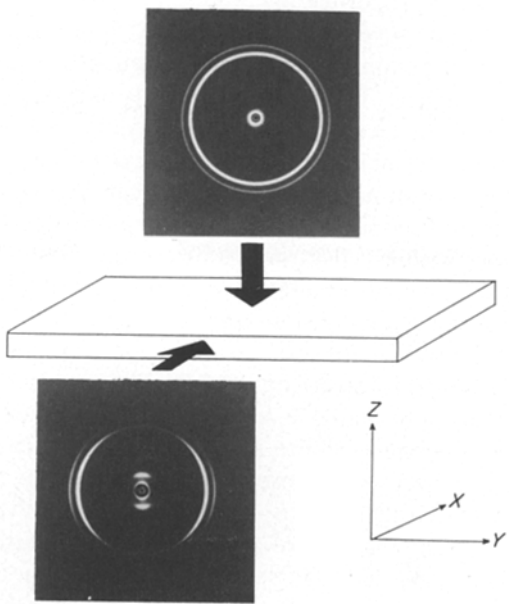

Figure 1 Combined WAXS and SAXS patterns of a dried UHMW-PE gel film. The arrows indicate the direction of the primary beam used. Note that the sample to film distance is different for both WAXS and SAXS.

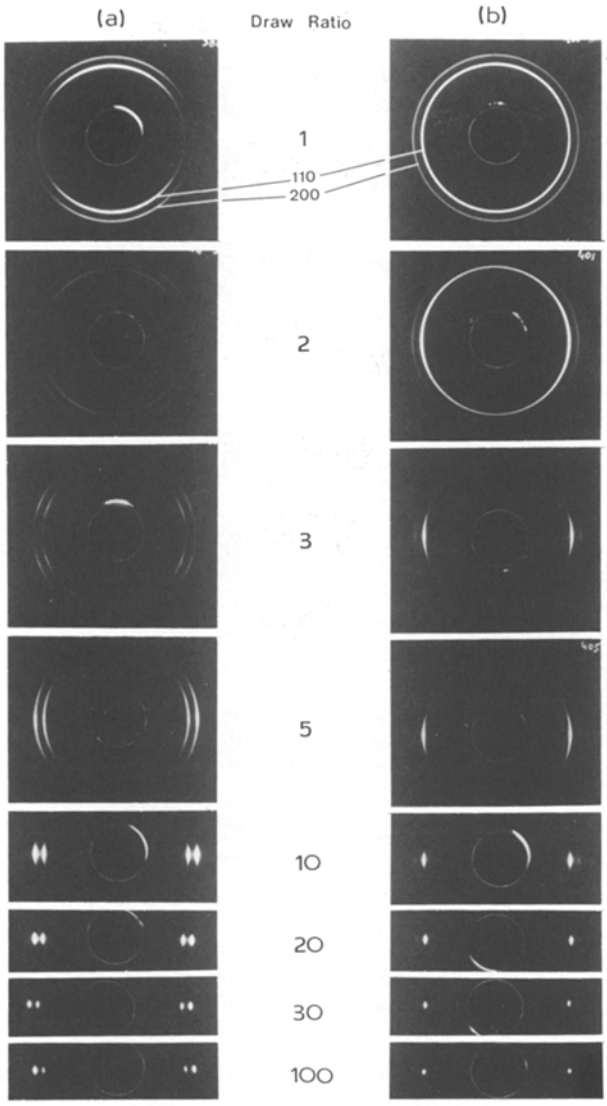

Figure 2 WAXS patterns of UHMW–PE gel tapes stretched at 120° C to the draw ratios indicated. (a) obtained with the primary beam parallel to the tape surface, (b) with the beam perpendicular to the tape surface. The drawing direction is vertical.

3.2.1. WAXS

Some characteristic WAXS patterns are presented in Fig. 2. From these data it can be concluded that the crystallized molecules orient towards the drawing direction during the drawing process. The WAXS data obtained with the incident X-ray beam parallel to the tape surface (Fig. 2a) show the existence of two preferential orientations in the necking region (draw ratio between 1.2 and 5), since the orthorhombic (1 1 0) and (2 0 0) reflections split into two arcs on both sides of the equator. The angle between the mean molecular chain orientation and the drawing direction decreases from 90° to 0° within the necking region. After necking this angle has become 0° and the resulting single arc of the reflections decreases during further drawing.

The WAXS data obtained with the incident X-ray beam perpendicular to the tape surface (Fig. 2b) show a smooth changing of the average molecular chain orientation. In contrast to the WAXS data of Fig. 2a both the (1 1 0) and the (2 0 0) reflections almost immediately intensify as arcs on the equator. As the draw ratio increases, the reflection arcs decrease, indicating an increase in molecular orientation. The orientational changes are quite different from those presented in Fig. 2a, especially at low draw ratios. Furthermore, notice the remarkable intensity difference for the (1 1 0) and (2 0 0) reflections as measured with the X-ray beam directed in different ways with respect to the tape surface. This is already easily detectable at draw ratios of 3 and higher.

Higher order reflections were recorded at a smaller sample to film distance. Some results are shown in Fig. 3 for a tape drawn to a draw ratio of 100. Besides the aforementioned intensity difference of the (1 1 0) and (2 0 0) reflections, also a striking difference for the (0 2 0) reflection can be seen. In addition, the presence of reflection spots with a corresponding d value of 0.455 nm assigned to an oriented triclinic crystal structure [27] is detected, with the intensity of the (0 1 0) reflection being clearly dependent on the direction of the incident beam with respect to the tape surface.

The apparent crystal sizes (ACS) along three lattice directions (2 0 0, 0 2 0 and 1 1 0) were determined with the incident X-ray beam perpendicular to the tape surface. The results, as presented in Fig. 4, show that the ACS decrease rather drastically during the initial stages of drawing. As the draw ratio exceeds 30, further drawing leads to a subsequent small increase.

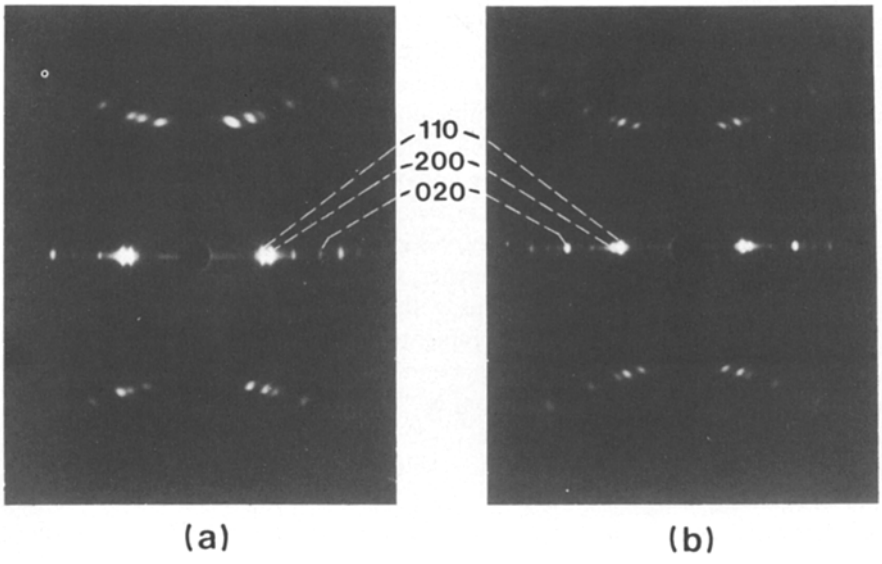

Figure 3 WAXS patterns of an UHMW–PE tape, drawn to a draw ratio of 100 at 120° C, obtained with the primary beam parallel (a) and perpendicular (b) to the tape surface. The drawing direction is vertical.

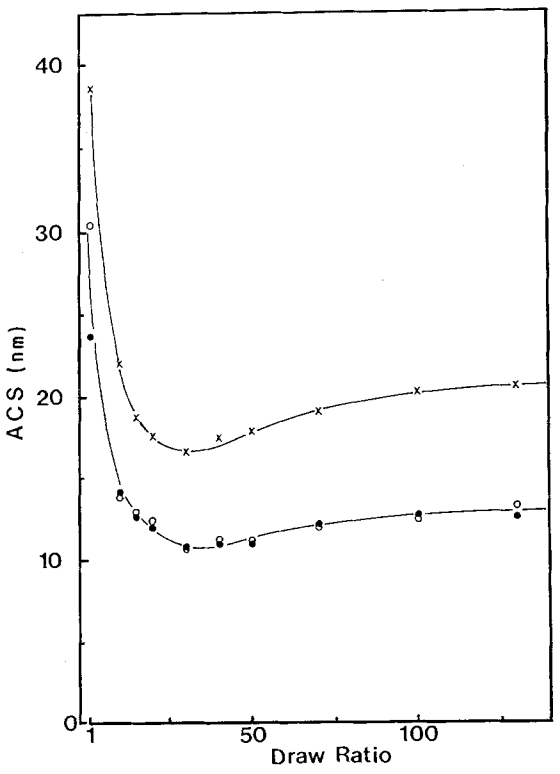

Figure 4 ACS (apparent crystal sizes) along the (1 1 0) (x), (2 0 0) (●) and (0 2 0) (○) directions as a function of the draw ratio.

Furthermore it should be noted that the ACS along the (2 0 0) and (0 2 0) direction coincide within the experimental error. This indicates the absence of differences in ACS behaviour along the *a* axis and *b* axis, despite the presence of strongly preferential orientation of both axes within the tape.

3.2.2. SAXS

From the SAXS data, which are presented in Fig. 5a, it can be seen that the long period also changes its preferred orientation towards the drawing direction. Like the WAXS data, the SAXS data show the biggest reorientation processes taking place within the small necking region.

For the sake of clearness the SAXS results obtained with the incident beam parallel to the tape surface (Fig. 5a) are presented schematically in Fig. 5b. Notice the transformation of the initial pattern (i.e. the undrawn material) via a four-point diagram (at a draw ratio of 3–4) into a pattern with long range order parallel to the drawing direction (at a draw ratio of 10). During the first stages of drawing a combination of the initial and the intermediate pattern can be detected. In addition, the angle between the maxima of the four-point pattern and the drawing direction changes gradually from about 70° at a draw ratio of 2 to approximately 10° at a draw ratio of 5. Upon further drawing the intensity of the first-order maximum decreases, while streak formation occurs at the first and zero order maxima.

The SAXS data presented in Fig. 5c were obtained with the incident beam perpendicular to the tape surface. As in the case of the WAXS results, the SAXS results are highly dependent on the relative direction of the incident beam at low draw ratios. It is clear that there is a weak first-order maximum parallel to the

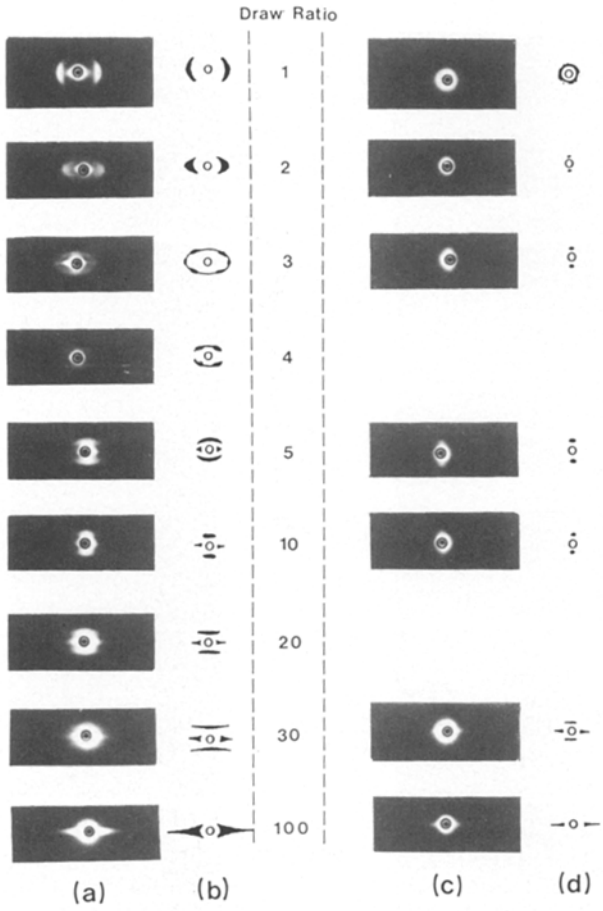

Figure 5 Observed and schematical representations of SAXS patterns, obtained for UHMW-PE gel tapes, stretched at 120° C to the draw ratios indicated. The drawing direction is vertical and the primary beam was directed parallel (a, b) and perpendicular (c, d) to the tape surface.

drawing direction already during the first stages of drawing (i.e. at a draw ratio of 2). This first-order maximum cannot be detected anymore at high draw ratios with the camera used. Furthermore, the streak formation as mentioned before is less pronounced and only detectable at the equator.

Since the Kiessig camera used has a limited resolution (about 25 nm) a Kratky camera was used to determine accurate values for the long period (L). The scattering patterns of Fig. 5c, d show perfect orientation of the first-order maxima at all stages of drawing, implying that the scattering curves obtained with a Kratky camera in which the samples are placed with their drawing direction exactly perpendicular to the slits of the camera and the incident beam perpendicular to the sample surface are implicitly desmeared. The Kratky SAXS patterns obtained are measured and corrected for liquid scattering, sample thickness and fluctuations in the intensity of the primary beam. In this way all curves were recalculated to the same intensity scale. Further, scattered intensities measured with the apparatus without any sample were subtracted from the aforementioned corrected intensities. As can be seen in an example (Fig. 6) this procedure enables determination of long period characteristics from scattering curves even with weak first-order maxima. Finally, some results are presented in Fig. 7 . Besides the variation of L, drastic intensity changes of the first-order maxima can be noticed. SAXS intensity

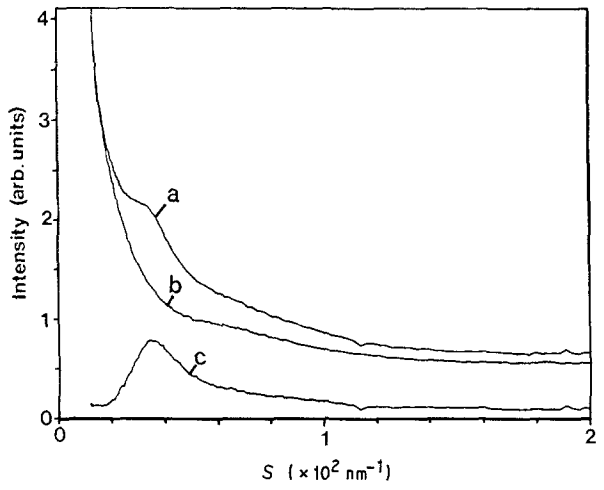

Figure 6 Correction of meridional SAXS intensity curves of an UHMW–PE tape of draw ratio 30. (a) observed SAXS curve for the sample, (b) intensity curve without any sample (i.e. background), (c) corrected SAXS intensity curve for the sample. $S = 2 \sin \theta/\lambda_x$.

caused by the presence of a long period can be detected in this way for draw ratios up to 40. Despite the strong changes in intensity, the long period L does not change for draw ratios of 10 and higher.

4. Discussion

4.1. Undrawn gel

The X-ray results of the undrawn material described in Section 3.1 point to the existence of lamellar crystals, as has been confirmed in the past by TEM experiments [28]. The preferred orientation in the cast and dried gel has already been described by Smith *et al.* [7]. Similar phenomena are also observed for single crystal mats, obtained by slow filtering of a suspension of single crystals or by sedimentation [29–33]. In the case of single crystal mats the orientation is caused by a combination of gravity and flow effects during the filtering. In cast gels, however, the orientation is caused by the drying procedure. A cast film tends to shrink in all directions during drying. The solvent can be removed by extraction with a low boiling solvent such as hexane, or by evaporation. In the extracted gel films as well as in the unconstrained dried films no preferred orientation was observed. However, when the cast film was clamped during the drying procedure, in order to avoid shrinking of the sample, preferred orientation was introduced. No difference in orientation was found when the clamped film was horizontally or vertically positioned during drying. This implies that only shrinking forces and not gravity effects are responsible for the occurrence of the initial orientation.

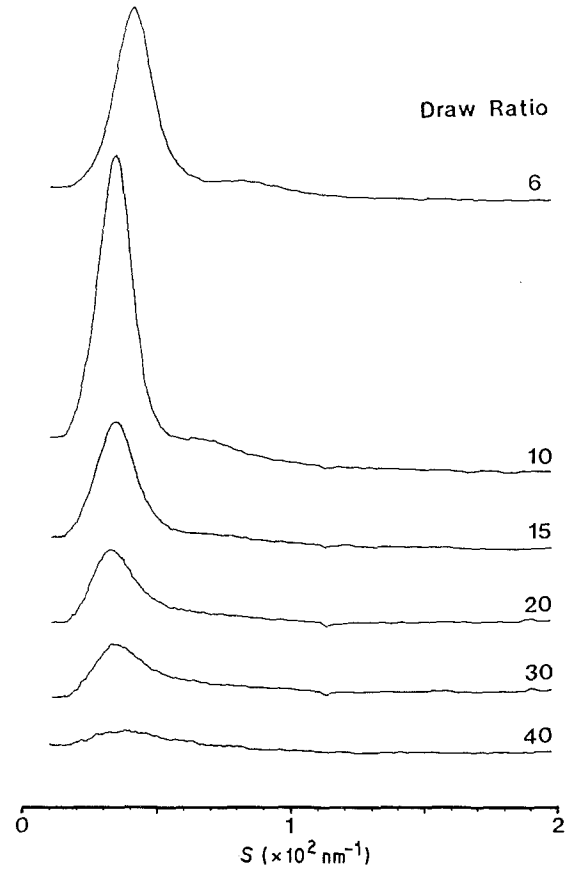

Figure 7 Corrected meridional SAXS curves of UHMW–PE tapes, stretched at 120° C to the draw ratios indicated. $S = 2 \sin \theta/\lambda_x$.

4.2. Drawn gel

4.2.1. Structure at low draw ratios

The WAXS and SAXS results obtained at low draw ratios by irradiation parallel to the tape surface can be described and understood completely with the deformation model originally described by Peterlin [10, 11]. This model describes the transformation of lamellar into fibrous structures at low draw ratios via chain tilting, slipping and twisting. The presence of preferentially oriented lamellae enables us to follow the deformation process of these lamellae from aside and from the top of the lamellae. The results presented are to a very high degree similar to those obtained for single crystal mats [29, 30]. This is also true for higher-order reflections, not shown here. It is not surprising, since the initial structure of such mats does not differ much from solution cast gel films. Furthermore, the results are also quite similar to those obtained for linear low molecular weight PE drawn at elevated temperatures to draw ratios between 1 and 6 [34, 35]. Finally it should be mentioned here that during the lamella–fibril transformation no melting into a randomized melt can occur, as suggested by Juska and Harrison [20, 21], since in that case no differences should be observable in WAXS and SAXS patterns obtained with the X-ray beam parallel or perpendicular to the tape surface after this transformation.

4.2.2. Structure at high draw ratios

After the structural reorganisation (i.e. at a draw ratio above 5) the samples show a high degree of orientation, as illustrated by the WAXS data in Fig. 2. Further drawing reduces the deviation from the preferred orientation. At draw ratios above 30 hardly any improvement of chain orientation can be detected. At extremely high draw ratios (above 80) the samples seem to be perfectly oriented and crystalline. These results are in excellent agreement with data of Smith and Lemstra [2]. However, an accurate investigation of these diffraction patterns still reveals the presence of traces of an amorphous fraction as was clearly observable on the original photographs (Fig. 3).

From the SAXS results presented in Fig. 7, the

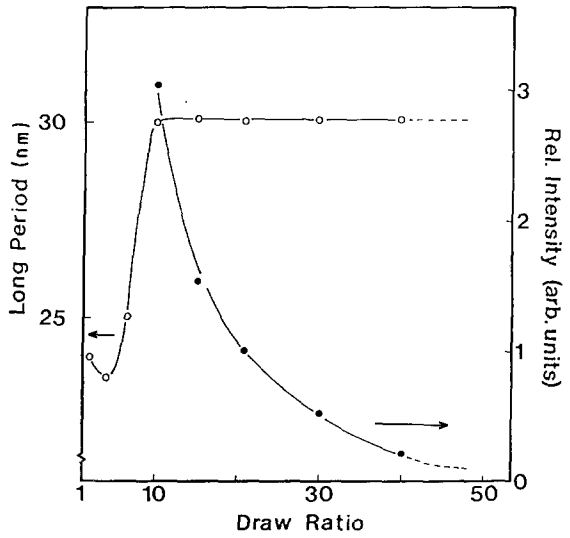

Figure 8 Influence of draw ratio on the long period (○) and the integral intensity of the Bragg-peak (●).

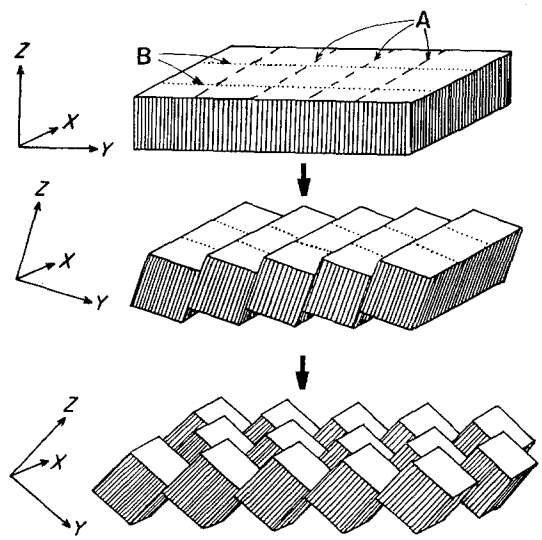

Figure 9 Schematical representation of the lamellar break-down during the initial stages of drawing. (A) cleavage planes, giving rise to intra-microfibrillar tie-molecules, (B) cleavage planes giving rise to inter-microfibrillar tie-molecules. The Z axis indicates the preferential c axis orientation at each stage of drawing.

dependency of L and the integral intensity of the Bragg peak on the draw ratio can be obtained. These dependencies are presented in Fig. 8. As mentioned in the preceding paragraph, the structural changes caused by the drawing, up to a ratio of about 10, can be understood in terms of the deformation model presented by Peterlin. At higher draw ratios the intensity of the long period decreases drastically, whereas the value of L remains constant. These results are similar to experimental data obtained for drawn melt-crystallized commercial linear PE grades [36, 37]. This implies that the molecular weight and the use of gelation has no significant influence on the behaviour of the long period upon drawing. Since, even at a draw ratio of 40, the above-mentioned integral intensity deviates from zero, some amorphous material must be present.

Clements and Ward [37] explain the observed decrease in SAXS reflection intensity at higher draw ratios by an increase in formation of crystalline bridges acting as links between oriented lamellae. Peterlin and Corneliussen [36] ascribe it to a decrease of effective electron-density difference between amorphous and crystalline components. However, the above-mentioned interpretations are not simply transferable to deformations up to extremely high draw ratios. Our results can be easily understood by a deformation model which is more or less an extension of the model originally described by Peterlin, as will be shown in the next paragraph.

4.3. Extended deformation model

The transformation of lamellae into microfibrils has been described in detail in the past [10–12]. This transformation starts with a breaking of lamellae into smaller units, accomplished via the initiation of two kinds of cleavage planes. A schematical representation is given in Fig. 9, in which the Z axis represents the molecular chain direction. During the drawing process larger blocks of folded chains are broken off from the lamellae and incorporated into so-called microfibrils. If the cleavage plane A (i.e. plane XZ in Fig. 9) is not parallel to the growth plane, many molecular folds will cross this cleavage plane. These folds will be translated axially and withdrawn from the lamellar parts. In this way microfibrils are formed in which crystallites are stacked and connected by so-called intra-microfibrillar tie-molecules (intra-TMs). These intra-TMs arise from the molecular folds that originally bridged the A-cleavage planes and thus originate from the same lamella.

Besides the intra-TMs, a second type of tie-molecules will be introduced during the microfibril formation. Just after the formation of the fibrillar texture, the microfibrils are connected laterally by bridging molecules, which are called inter-microfibrillar tie-molecules (inter-TMs). Since microfibrils are formed out of lamellar parts, which are separated via cracking planes B, parallel to the drawing direction (i.e. planes YZ in Fig. 9), the inter-TMs must originate from molecules which were originally bridging the cracking planes or from inter-lamellar tie-molecules. For the sake of simplicity the formation of both kinds of cleavage planes (A and B) is presented as two independent processes. Of course we are well aware of the fact that both processes may occur more or less simultaneously.

Just after the lamella–fibril transformation, during which the different types of microfibrillar tie-molecules (TMs) are introduced, further drawing first leads to a tautening of the intra-TMs. This process can be followed experimentally via the increasing L value (see Fig. 7 and 8). The tautening of the intra-TMs is completed at a draw ratio of about 10, as can be deduced from the constancy of the L value after that point. Furthermore, during these initial stages of the plastic deformation, the microfibrils are also translated with respect to each other, resulting in a tautening of the inter-TMs. Due to this tautening, the inter-TMs will bridge an increasing amount of alternating crystalline-amorphous blocks of the microfibrils.

Further drawing leads to the pulling out of inter-TMs out of the microfibrils via unfolding of microfibrillar

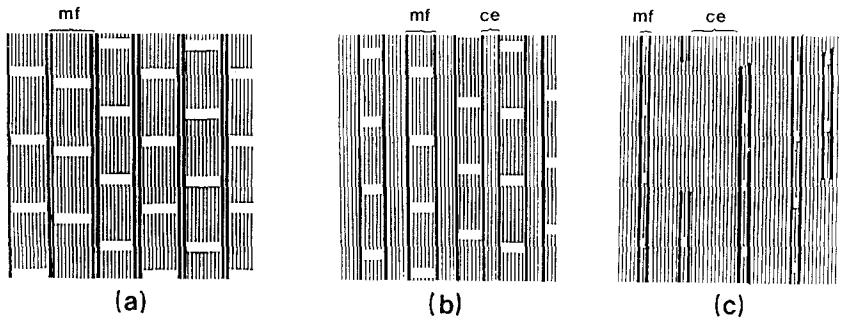

Figure 10 Schematical representation of three stages of plastic deformation. The bold and the thin lines represent the microfibril boundaries and the molecular chain directions respectively. The white regions indicate the amorphous material. During the deformation process the microstructure will change gradually from structure (a) to (c) via a transformation of microfibrils (mf) into more or less chain-extended material (ce).

crystallites, resulting in a decreasing microfibrillar fraction and an increasing fraction of inter-microfibrillar material. The latter fraction will consist of molecules with increasing stem lengths, finally leading to extended chains (Fig. 10).

Now it can be easily understood why the value of L remains constant for draw ratios above 10. Also the decrease of the SAXS intensity can be explained by the decrease of the microfibrillar fraction during the drawing process, since the microfibrils form the exclusive fraction with alternating electron densities and therefore the only fraction responsible for the meridional SAXS intensity. The growing chain-extended fraction will lead to a larger average crystal size in the drawing direction, although L will remain constant. The experimental data of Clements and Ward [37] are in this way easily explained. The observed increase in crystallinity as a function of the draw ratio (see e.g. [2]) can also be explained very easily in terms of this model. Since most of the amorphous material is part of the microfibrils, a decrease of the microfibrillar fraction will unavoidably lead to a simultaneous decrease in amorphous material and thus in an increase in crystallinity.

The above-described molecular deformation model also easily explains the variation of the ACS shown in Fig. 4. At draw ratios below 5 the cleavage of chain-folded crystals (lamellae) into microfibrils will reduce the lateral crystal dimensions. As the drawing proceeds, the lateral dimension of the microfibrils will decrease due to the process of unfolding into chain-extended material. In this way the mean lateral dimension of the chain-extended fraction increases at the expense of the microfibrillar fraction. At intermediate draw ratios (i.e. between 5 and 40) the experimental ACS are average values of the lateral dimensions of the decreasing microfibrillar fraction and the increasing chain-extended fraction. At draw ratios above 40 the microfibrillar fraction is reduced to such an extent that its contribution to the observed crystal sizes becomes negligible. Hence the observed increase in crystal sizes at draw ratios above 30 can be understood in terms of an increase in the mean value of the lateral dimensions of the chain-extended fraction.

Furthermore, this deformation model can be used to describe the shape of the stress–strain diagram of drawing, i.e. the constancy of the engineering stress for solution cast PE-films (e.g. see Fig. 1 of Smith *et al.* [6]). After the formation of microfibrils and the tautening of all TMs, the only deformation will be the unfolding of molecular segments within the microfibrils, leading to an increase in chain-extended fraction. If the segments that will be unfolded arise from crystals in which the molecules are nicely adjacent re-entered, the absolute number of inter-TMs within an arbitrary cross-section of the sample will not change during the drawing process. Thus the applied stretching force for unfolding will not change very much, since the number of segments to be unfolded will be constant. As long as the possibility to unfold adjacent re-entered stems exists, this drawing process continues without a large increment in stretching force.

Let us define molecular clusters consisting of adjacent re-entered stems, which are randomly distributed amongst the microfibrils. When the unfolding of several of these clusters is more or less completed, further drawing will require an increasing stretching force and will therefore soon lead to sample failure, if the stretching force rises above the tensile strength of the weakest point of the sample. At this moment the maximum draw ratio is reached.

From the above, it follows that during the complete deformation process the cores of the individual clusters are never deformed, they are only displaced with respect to each other. Therefore, these centres can be considered as virtual constraining points (cross-links) during the complete drawing experiment. So the maximum draw ratio will depend on the average molecular weight M_a between two constraining points. M_a is influenced by the crystallization conditions. Melt-crystallization will lead to a small M_a whereas gelation from an extremely dilute solution, M_a will be maximal (single crystals). In semi-dilute solution the value of M_a will range between these two extremes. In a forthcoming paper [38] it will be shown that the relation between the maximum draw ratio and the concentration of the solution is equivalent to the relation

$$\lambda_{max} = \lambda^{1}_{max}\, \phi^{-1/2} \qquad (3)$$

as already described by Smith [39], where λ^{1}_{max} refers to the maximum draw ratio of melt-crystallized material and ϕ to the polymer volume fraction of the initial solution.

4.4. Final remarks

The observed three-dimensional anisotropy of the triclinic phase in the drawn tapes is caused by the anisotropy present in the initial undrawn gel. The relation between the anisotropy of the orthorhombic and triclinic PE phase was reported in the literature [40] and will not be discussed further.

All the above-presented X-ray results were obtained

for tapes drawn at elevated temperature but studied at room temperature. This implies that the results are not by definition representative of the deformation occurring *during* the deformation process itself. However, preliminary results obtained via real-time X-ray studies *during* the drawing process confirm the results described here [41].

5. Conclusions

The deformation of solution-crystallized UHMW-PE gels was studied via different X-ray techniques. The results imply a three-stage deformation process, analogous to Peterlin.

(1) Transformation of the lamellae into microfibrils during the initial stages of drawing (similar to the model described by Peterlin).

(2) Tautening of the inter- and intra-microfibrillar tie-molecules, introduced during the first stage.

(3) Unfolding of microfibrillar crystallites and addition of the resulting unfolded segments to the chain-extended fractions (the original inter-microfibrillar tie-molecules).

This model not only explains the orientational effects observed via WAXS and SAXS but also the constancy of the long period, the decrease of the meridional SAXS intensity, the increase in crystallinity, the changes in apparent crystal sizes and observed stress–strain behaviour.

Furthermore, the maximum achievable draw ratio can be understood in terms of the distribution of molecules amongst clusters, consisting of more or less adjacent re-entered stems.

Acknowledgements

The authors wish to thank Professor P. Lemstra (Eindhoven University of Technology), Dr B. Scholtens and Mr C. Bastiaansen (DSM-Research) for stimulating discussions and valuable comments. Furthermore, they gratefully acknowledge Mr W. Ramaekers (DSM-Research) for valuable experimental advices and support. This study was supported by DSM-Research.

References

1. P. SMITH, P. J. LEMSTRA, B. KALB and A. J. PENNINGS, *Polym. Bull.* **1** (1979) 733–6.
2. P. SMITH and P. J. LEMSTRA, *J. Mater. Sci.* **15** (1980) 505–14.
3. *Idem, Makromol. Chem.* **180** (1979) 2983–6.
4. *Idem, Polymer* **21** (1980) 1341–3.
5. *Idem, Colloid Polym. Sci.* **258** (1980) 891–4.
6. P. SMITH, P. J. LEMSTRA and H. C. BOOIJ, *J. Polym. Sci., Polym. Phys. Ed.* **19** (1981) 877–88.
7. P. SMITH, P. J. LEMSTRA, J. P. L. PIJPERS and A. M. KIEL, *Colloid Polym. Sci.* **259** (1981) 1070–80.
8. H. D. CHANZY, P. SMITH, J.-F. REVOL and R. St. J. MANLEY, *Polym. Commun.* **28** (1987) 133–6.
9. K. KOBAYASHI, in "Polymer Single Crystals" (edited by P. H. Geil) Wiley, New York (1963) p. 473.
10. A. PETERLIN, *J. Polym. Sci.* **C 9** (1965) 61–89.
11. *Idem, J. Mater. Sci.* **6** (1971) 490–508.
12. *Idem.*, "Advances in Polymer Science and Engineering" (edited by K. D. Pae, D. R. Morrow and Y. Chen) Plenum, New York (1972) pp. 1–19.
13. *Idem, Colloid Polym. Sci.* **253** (1975) 809–23.
14. *Idem, J. Appl. Phys.* **48** (1977) 4099–108.
15. *Idem,* "Ultra-High Modulus Polymers" (edited by A. Ciferii and I. M. Ward) Applied Science Publishers, London (1979) Chap. 10.
16. *Idem., Colloid Polym. Sci.* **265** (1987) 357–82.
17. E. W. FISCHER and H. GODDAR, *J. Polym. Sci.* **C 16** (1969) 4405–27.
18. E. S. CLARK and L. S. SCOTT, *Polym. Eng. Sci.* **14** (1974) 682–6.
19. P. J. FLORY and D. Y. YOON, *Nature* **272** (1978) 226–9.
20. T. JUSKA and I. R. HARRISON, *Polym. Eng. Rev.* **2** (1982) 13–28.
21. *Idem., Polym. Eng. Sci.* **22** (1982) 766–76.
22. G. D. WIGNALL and W. WU, *Polym. Commun.* **24** (1983) 354–9.
23. R. CORNELIUSSEN and A. PETERLIN, *Makromol. Chem.* **105** (1967) 193–203.
24. P. J. LEMSTRA, N. A. J. M. VAN AERLE and C. W. M. BASTIAANSEN, *Polym. J.* **19** (1987) 85–98.
25. C. G. VONK and A. P. PIJPERS, *J. Appl. Cryst.* **14** (1981) 8–16.
26. C. G. VONK, *ibid.* **8** (1975) 340–1.
27. A. TURNER-JONES, *J. Polym. Sci.* **62** (1962) S53-6.
28. C. W. M. BASTIAANSEN, P. FROEHLING, A. J. PIJPERS and P. J. LEMSTRA, "Integration of Fundamental Polymer Science and Technology" (edited by L. A. Kleintjens and P. J. Lemstra) Elsevier, London (1986) pp. 508–16.
29. K. ISHIKAWA, K. MIYASAKA and M. MAEDA, *Rep. Prog. Polym. Phys. Jpn* **11** (1968) 185–6.
30. K. ISHIKAWA, K. MIYASAKA and M. MAEDA, *J. Polym. Sci.* **A-2 7** (1969) 2029–41.
31. M. MAEDA, K. MIYASAKA and K. ISHIKAWA, *ibid.* **8** (1970) 355–70.
32. T. KANAMOTO, A. TSURUTA, K. TANAKA, M. TAKEDA and R. S. PORTER, *Rep. Prog. Polym. Phys. Jpn* **26** (1983) 347–50.
33. K. FURUHATA, T. YOKOKAWA and K. MIYASAKA, *J. Polym. Sci.: Polym. Phys. Ed.* **22** (1984) 133–8.
34. G. MEINEL, N. MOROSOFF and A. PETERLIN, *J. Polym. Sci.* **A-2 8** (1970) 1723–40.
35. A. PETERLIN and G. MEINEL, *Makromol. Chem.* **142** (1971) 227–40.
36. A. PETERLIN and R. CORNELIUSSEN, *J. Polym. Sci.* **A-2 6** (1968) 1273–82.
37. J. CLEMENTS and I. M. WARD, *Polymer* **24** (1983) 27–9.
38. B. J. R. SCHOLTENS and A. W. M. BRAAM, submitted to Colloid Polym. Sci.
39. P. SMITH, *Macromolecules* **16** (1983) 1802–3.
40. H. KIHO, A. PETERLIN and P. H. GEIL, *J. Appl. Phys.* **35** (1964) 1599–1605.
41. N. A. J. M. VAN AERLE and A. W. M. BRAAM, submitted to *Colloid Polym. Sci.*

Received 21 October 1987
and accepted 17 February 1988